
# Identifying the boundaries of sinkholes and subsidence areas via trenching and establishing setback distances

Francisco Gutiérrez, Mario Zarroca, Rogelio Linares, Carles Roqué, Domingo Carbonel, Jesús Guerrero, James P. McCalpin, Xavier Comas, Anthony H. Cooper

PII: S0013-7952(17)31104-3
DOI: doi:10.1016/j.enggeo.2017.12.015
Reference: ENGEO 4727

To appear in: *Engineering Geology*

Received date: 29 July 2017
Revised date: 23 November 2017
Accepted date: 21 December 2017

Please cite this article as: Francisco Gutiérrez, Mario Zarroca, Rogelio Linares, Carles Roqué, Domingo Carbonel, Jesús Guerrero, James P. McCalpin, Xavier Comas, Anthony H. Cooper , Identifying the boundaries of sinkholes and subsidence areas via trenching and establishing setback distances. The address for the corresponding author was captured as affiliation for all authors. Please check if appropriate. Engeo(2017), doi:10.1016/j.enggeo.2017.12.015

# Identifying the boundaries of sinkholes and subsidence areas via trenching and establishing setback distances

Francisco Gutiérrez (1)*, Mario Zarroca (2), Rogelio Linares (2), Carles Roqué (3), Domingo Carbonel (1), Jesús Guerrero (1), James P. McCalpin (4), Xavier Comas (5), Anthony H. Cooper (6)

(1) Departamento de Ciencias de la Tierra; Universidad de Zaragoza; C/. Pedro Cerbuna 12; 50009 Zaragoza; Spain; Phone: 34 976 761090

(2) Departamento de Geología; Universidad Autónoma de Barcelona; E-08193 Barcelona; Spain

(3) Àrea de Geodinàmica Externa i Geomorfologia; Universitat de Girona; Campus Montilivi; E-17003 Girona; Spain

(4) Geo-Haz Consulting Inc., CO, USA

(5) Department of Geosciences, Florida Atlantic University, Davie, FL, USA

(6) Independent geological consultant, formerly British Geological Survey, UK

*Corresponding author e-mail: fgutier@unizar.es

**Abstract**

One of the most effective mitigation strategies in sinkhole areas is the exclusion of sinkholes and their vicinity to construction. The application of this preventive measure requires precise mapping of the boundaries of the areas affected by subsidence and the establishment of adequate setback distances, which is an important policy issue with significant economic implications. Through the investigation of several buried sinkholes in the mantled evaporite karst of the Ebro Valley by trenching, this work illustrates that the actual extent of the subsidence areas may be much larger than that inferred from surface mapping and geophysical surveys. The objective and accurate subsurface information acquired from trenches on the outer edge of the deformed ground revealed sinkhole radii 2-3 times larger than initially estimated, increasing one order of magnitude the sinkhole area. Trenches can therefore help to reduce mapping uncertainties and the size of setbacks. Moreover, the trenching technique, in combination with geochronological data and retrodeformation analyses, provides critical information on the subsidence phenomena and the characteristics of the sinkholes relevant to hazard assessment. Since recommended setback distances found in the existing literature are highly variable and rather arbitrary, we include a discussion here on the main factors that should be considered when defining setback for sinkholes.

**Key words:** Sinkhole mapping; hazard zonation; planning; retrodeformation analysis; geophysics

## 1. Introduction

Over the last few decades, sinkhole hazards and their associated risks have increased dramatically in many inhabited areas (e.g., Waltham et al., 2005; Gutiérrez et al., 2014). Despite the advances in our understanding of sinkholes revealed by the rapidly increasing scientific production, commonly there is no efficient transfer of knowledge and needs between scientists, technicians and decision-makers. This frequently leads to unproper planning and risk management, resulting in significant economic losses (Gutiérrez, 2016 and references therein). Nonetheless, there is an emerging trend in many karst regions to incorporate sinkhole hazards in land-use planning (e.g., Farrant and Cooper, 2008). An essential step for risk mitigation in sinkhole areas is the construction of comprehensive and accurate cartographic sinkhole inventories. These maps and their data allow the identification of the areas affected by subsidence and delineation of the most hazardous sectors. Preventive planning is probably the safest mitigation strategy, which is typically implemented through regulations that exclude sinkholes and their vicinity from development and various anthropogenic activities. The effective application of this "hazard avoidance" measure requires: (1) the identification of all the existing sinkholes; (2) precise mapping of the edges of the sinkholes and the underlying subsidence structures; and (3) the definition of an adequate setback distance from the sinkhole edge. Mapping the boundaries of sinkholes and the areas affected by subsidence is frequently a challenging task and may have a high degree of uncertainty due to the following reasons: (1) the geomorphic expression of sinkholes is commonly obliterated or subdued by anthropogenic filling and natural depositional and erosional processes; (2) some depressions may have an uncertain origin and may be related to non-karstic processes (artificial excavation, aeolian deflation); (3) the actual area affected by subsidence may be smaller than the topographic depressions due to recession of the edges by erosion and the consequent expansion of the topographic basin (e.g., Fabregat et al., 2017) (**Fig. 1A**); and (4) the area affected by ground settlement may be much larger than the apparent size of the sinkhole mapped on the basis of surface evidence (e.g., Pueyo-Anchuela et al., 2013; Carbonel et al., 2014). This underestimation of the sinkhole size is frequently related to subtle subsidence at the sinkhole margins with little topographic expression, a situation common in complex sagging and collapse sinkholes (**Fig. 1B**).

Once the boundaries of the sinkholes or subsidence areas have been mapped, the next step is to establish a setback distance to define a potentially hazardous zone where infrastructure construction and certain activities that should be avoided. The size of the setback distance is an important policy issue with significant economic implications. A large setback distance contributes to protect the population from sinkhole damage but causes: (1) land devaluation at the problem site; (2) reduction of the area suitable for construction; and (3) increased housing value in the area (Smith, 1994). A compromise should be found between the benefits of the setback zone for preventing subsidence damage and its detrimental impacts on property value.

The setback concept has been applied for managing a number of geo-environmental problems. It is frequently used to define zones that may be affected by hazardous processes spatially associated with mappable geological or geomorphological features including: (1) ground ruptures related to active faults (McCalpin, 1987; Bryant, 2010; Zhou et al., 2010; Boncio et al., 2012); (2) surface deformation and deposition in the vicinity of landslides; (3) erosion at the banks of a migrating fluvial channel; (4) flooding and erosion by severe waves in coastal areas (e.g., Gibb, 1995); and (5) subsidence at the margins of sinkholes (Zhou and Beck, 2008; Fleury, 2009). The approaches used to define setback distances are highly variable and may include the statistical analysis of past events, the assessment of trends from historical and instrumental data, the consideration of different temporal horizons through magnitude and frequency relationships, or the provision for the effects of future scenarios (e.g., sea-level rise).

The setback concept is also employed for preventing or ameliorating the impact of some human activities on the geological environment: (1) minimize restriction of channel migration and cutoff to allow the development of ecologically valuable fluvial environments (Larsen et al., 2006); (2) protect karst aquifers from pollution by an exclusion zone around sinkholes (Paukstys et al., 1999). In Minnesota, any liquid manure storage is prohibited within 91 m from the outside edge of sinkholes (Minnesota Pollution Control Agency, 2000).

Previous papers dealing with the application of the trenching technique to sinkhole investigation are focused on several aspects related to the subsidence phenomena relevant to hazard assessment, such as subsidence mechanisms and kinematics,

subsidence rates, timing of subsidence events and recurrence (Carbonel et al., 2014; Fabragat et al., 2017; Sevil et al., 2017). The aim of this paper is to illustrate, through the application of the trenching method (1) the significant mismatch that may exist between the actual boundaries of the areas affected by subsidence in sinkholes and the edges of the corresponding topographic depressions; (2) the practicality of the trenching technique for accurately and unambiguously locating the boundaries of the unstable areas affected by ground subsidence, in comparison with other methods like surface mapping or shallow geophysics (GPR, ERI); (3) the value of information that can be extracted from trenches relevant to hazard analysis, in combination with geochronological data and retrodeformation analyses. This work also discusses some of the criteria that may be considered for the establishment of setback distances around sinkholes. These concepts and approaches, relevant to sinkhole hazard assessment and risk management, are explored through the investigation of three buried sinkholes located in urban and suburban areas located on the mantled evaporite karst of the Ebro River valley, in and around the city of Zaragoza, NE Spain (**Fig. 2**).

## 2. Methodology

The sites of the buried-sinkholes were mapped using several approaches before conducting the trenching investigations. Old aerial photographs from different dates, interpreted using a stereoscope, allowed us to identify some of the depressions before they were obliterated by anthropogenic infill. Some of the aerial photographs were also orthorectified and georeferenced with ArcGIS 10.3 to approximately locate the interpreted subsidence depressions. A topographic map from 1969, produced at a scale of 1:2000 and with contour interval of 1 m, allowed the recognition of the Ventas sinkhole, obliterated by man-made deposits. Subsequently, the sites were mapped in the field using large-scale gridded orthoimages. The positioning of surveyed features on the orthoimages was carried out using metric tape, and eventually a hand-held GPS, always with a horizontal accuracy lower than 3 m. Special attention was paid to sinkhole-related deformation observed on the ground surface and visible in human structures (e.g., cracks, scarps, tilting, sags). These features provide useful information on the area affected by active subsidence, as well as the amount and sense of displacement.

The airport-road sinkhole was investigated by means of Electrical Resistivity Imaging (ERI) and Ground Penetrating Radar (GPR) before applying the trenching technique. The ERI section, the GPR profile presented in this work, and the trenches were located along the same line for direct comparison. A 126 m long ERI section was acquired across the sinkhole with a multi-electrode Lund Imaging System (ABEM) using an inter-electrodic spacing of 2 m. The system comprised a Terrameter SAS 4000 resistivitymeter, an ES10-64 electrode selector, 4 signal cables and reels and 64 steel electrodes. We selected a dipole-dipole electrode array which offers dense horizontal data saturation, high-sensitivity to lateral changes in resistivity (that occur in vertical structures expected in sinkhole areas), and moderate-sensitivity to vertical resistivity variation (Dahlin and Zhou, 2004). The measured apparent resistivity data were processed using the 2D inversion commercial software RES2DINV, based on the smoothed least-squares inversion of Loke and Barker (1996). The model grid was corrected by the topographic curvature by a damped distortion with depth. The topography was recorded using a Sprinter-100 (Leica) digital level.

The GPR data were collected with a RIS system (Ingegneria dei Sistemi) equipped with a 100 MHz shielded antenna, using a trace interval of 0.2 m and a sampling ratio of 512 scans. Post-processing of GPR data was completed with ReflexW (by Sandmeier Scientific) and included the following steps: 1) substract-mean dewow (10 ns); 2) background removal; 3) manual gain; 4) bandpass frequency; 5) Stolt migration using a single velocity of 0.09 m ns-1 estimated from diffraction hyperbolas; and 6) topographic correction.

Trenches were excavated with rubber-tired backhoes. After cleaning the walls, a reference grid was installed with strings on one of the walls with a spacing 1 or 2 m. The selected wall, preferably the most shaded one, was logged on graph paper at a scale of 1:50. Samples were collected in one of the trenches for radiocarbon dating. The accelerator mass spectrometry (AMS) radiocarbon ages provided by Beta Analytic were calibrated using CALIB 7.1 and the data set IntCal 13 of Reimer et al. (2013) (**Table 1**).

## 3. Study area

The study area is located in middle reach of the Ebro River valley, in Zaragoza city and its surroundings, NE Spain (**Fig. 2**). From the geological perspective, the area is situated in the central part of the Ebro Cenozoic Basin. The bedrock corresponds to the horizontally-lying Zaragoza Gypsum Formation. This is an Oligo-Miocene evaporitic succession more than 850 m thick deposited in playa-lake systems (Quirantes, 1978; Salvany et al., 2007). In the subsurface, the non-weathered evaporitic formation consists of anhydrite ($CaSO_4$), halite (NaCl) and glauberite ($Na_2Ca[SO_4]_2$) with interbedded shale and marl layers. In outcrops, the weathered zone of the evaporitic formation displays secondary gypsum ($Ca[SO_4]$ $2H_20$) related to the hydration of anhydrite and the incongruent dissolution of glauberite (Salvany et al., 2007). Recent borehole data reveal the presence of thick high-solubility halite and glauberite units at limited depth beneath the Quaternary alluvium (terraces, pediments). The rapid karstification of these salts plays an instrumental role in the development of dissolution-induced subsidence phenomena in the area (e.g., Guerrero et al., 2013; Gutiérrez et al., 2015). Data on the hydrogeological functioning of the karstic-alluvial aquifer system can be found in Acero et al. (2015).

Active sinkholes are common and tend to be associated with the floodplain and the lowermost terraces. They may be related to various subsidence mechanisms (sagging, collapse, suffosion) and show a wide range of dimensions, from around 1 m to hundreds of meters across. Detailed information of the subsidence mechanisms, inferred from the paleokarst, can be found in Gutiérrez et al. (2008a) and Guerrero et al. (2013). Many of those sinkholes were filled in the past and concealed by the construction of human structures such as roads, railways, buildings, industrial states (e.g., Galve et al., 2009). These obliterated depressions are responsible for a great part of the sinkhole damage in this area, considered to be the evaporite karst region in Europe with the highest sinkhole risk (Gutiérrez et al., 2008b). Identifying the existing sinkholes and precisely mapping their edges, rather than predicting new ones, is the most important step towards the application of effective mitigation measures in this region. This work is focused on three buried sinkholes located on terraces of the Ebro River and associated with human structures and development areas (**Fig. 2**): the airport-road and the Ventas sinkholes are situated in the lower terrace subject to irrigation and underlie the N-125 and N-232 roads, respectively. The Rosales sinkhole is located on a high terrace dissected by an

infilled valley, outside the irrigation area, but in a suburb of Zaragoza city that is undergoing urban expansion.

## 4. Airport-road sinkhole

### 4.1. Description of the site and investigation layout

This sinkhole is located at the right margin of the Ebro River valley, on the second terrace above the floodplain, which is perched 25-30 m with respect to the river channel (Galve et al., 2009) (**Fig. 2**). Currently, the sinkhole lies south and beneath the airport road (N-125) and causes progressive sagging in the infrastructure, which is built on an embankment (**Fig. 3**). The sinkhole is clearly identifiable in aerial photographs from 1946 (1:43,500 scale) and 1956 (1:32,500) as a funnel-shaped depression showing a well-defined edge with an E-W oriented ellipsoidal geometry 60 m long and 42 m wide. The sinkhole was filled between 1956 and 1970. Images from 1970, 2007 and 2017 capture re-asphalted sections of the road 20, 65, and 170 m long, respectively (**Fig. 3**). The area was surveyed with the aim of identifying surface evidence of deformation, including: (1) a sag in the road pavement with vaguely-defined edges and the deepest sector situated next to the central sector of the adjacent square-shaped plot of land; (2) a tilted pole of a power line; and (3) a tilted tree on the NW corner of the plot of land (**Fig. 3**).

The mapped evidence of ground subsidence suggests that the active and buried sinkhole covers a much larger area than the funnel-shaped depression identified in the aerial photographs taken in 1946 and 1956 (**Fig. 3**). In order to test this hypothesis and better characterise this damaging sinkhole, a site investigation was conducted combining non-intrusive near-surface geophysical methods and trenching. The geophysical survey comprised the acquisition of an ERI section and multiple GPR profiles with a 100 MHz shielded antenna. The 126 m long and NE-SW-oriented ERI section extended from the SW corner of the plot of land to the foot of the road embankment (**Fig. 3**). The resistivity line had to be confined to the uncultivated plot due to permit constraints and the presence of a road, but traversed the depression mapped in the old aerial photographs. A total of five GPR profiles were acquired within the square-shaped plot,

each around 101-120 m long, and with multiple orientations. For brevity and direct comparison with other methods, we only present the 101 m long GPR profile collected along the same line as the ERI section (**Fig. 3**). Furtheremore, the sinkhole was investigated by means of two trenches excavated along the NE-SW oriented line surveyed by ERI and GPR (**Fig. 4A**). Trench T1, 59 m long, covered the SW margin and edge of the buried depression identified in old aerial photographs. Trench T2 was sited on the northern edge of the depression and reached a length of 10 m (**Fig. 3**).

### 4.2. ERI and GPR profiles

The resistivity image shows two main electro-units with contrasting resistivity values (**Fig. 5B, C**). The upper low-resistivity unit, ascribed to the sinkhole fill, includes fine-grained deposits and extends from around 34 m to the NE end of the section. This conductive unit shows sharp thickness increases at 54 m and 114 m, roughly coinciding with the margins of the buried depression identified in old aerial photographs (**Fig. 3**). In the deeper area the sinkhole fill reaches 7-9 m in thickness. This should be considered as a minimum value since the ERI section was not acquired along the central axis of the funnel-shaped buried depression. The low-resistivity unit thins out at 54 m and towards the SW, and pinches out at 34 m. The underlying high resistivity layer, attributed to the gravely terrace deposit, is imaged right beneath the surface in the SW sector of the profile and plunges beneath the sinkhole fill NE of 34 m. This unit, noticeably deformed, shows a clear concentration of anomalous high resistivity nodes at around 60 m, coinciding with the sharp thickness increase in the sinkhole fill deposit and the corresponding vertical drop of the terrace gravels. A similar pattern is observed at 116 m, also spatially associated with the sharp thickness change in the sinkhole fill. These features may be interpreted as inversion artefacts related to collapse faults or fault zones (e.g., Zarroca et al., 2017; Fabregat et al., 2017). The ERI and geological sections shown in figure 5 illustrate the interpreted faults and fissures and their correspondence with those exposed in the trenches. The structures depicted SW of fault F2 would very difficult to identify without the direct data provided by the trenches.

The GPR profile shows two main regions with different reflection patterns (**Fig. 5A**). Between 40 and 96 m, coinciding with the location of the buried depression (**Fig. 3**), the profile shows lower penetration (3-4 m) and relatively continuous reflections with synformal geometry. These reflections, related to the sinkhole fill, apparently show upward dip attenuation at the NE margin of the basin. In the SW half of the sinkhole fill

the reflections are more irregular and laterally discontinuous. On both sides of the basin fill, the profile shows higher penetration in the terrace gravels (4-5 m) and is dominated by reflections dipping towards the synformal structure. The dipping reflections at the SW margin of the synformal structure, between 38-44 m, show a prominent vertical lateral truncation, a zone of highly irregular reflection and the apex of a diffraction hyperbola. On the opposite margin of the synform, between 96 and 100 m, the inward dipping reflections also display lateral truncation next to the apex of a diffraction hyperbola. The location of these features attributable to the margin of a collapse structure, and coincide with the inversion artefacts imaged in the ERI section.

Overall, the geophysical survey, in agreement with field observations, suggests that the airport-road sinkhole is a large sagging structure dominated by centripetal tilting (passive bending), with a collapse around 50 m across in the inner portion controlled by ring faulting. The ERI section provides a minimum value for the sinkhole fill thickness and the throw of the collapse structure, as it was not acquired along the deeper part of the depression.

### 4.3. Trenching

*Trench T1*

This trench, 59 m long, was excavated with a NE-SW orientation in the SW margin of the depression mapped on the aerial photographs from 1956 (**Figs. 4, 6**). The excavation started close to the SW corner of the square plot and it was stopped where it reached a thick and unstable man-made fill (**Fig. 3**). It exposed three sedimentary packages (I to III) overlain by a surficial horizon up to 0.5 m thick of agricultural soil disturbed by ploughing (S) (**Figs. 4B, 6**). See description of sedimentary units in **Figure 6**. The oldest package I corresponds to a pre-sinkhole terrace deposit overprinted in the upper part by a calcic horizon.

The intermediate package II, found NE of 29 m, is a natural sinkhole deposit comprising four stratigraphic units (II1 to II4) that reach a minimum thickness of 1.9 m. The units of this package thicken towards the NE, show an overall cumulative wedge-

out and an onlap arrangement between 29 and 45 m, recording an expansion of 16 m in the sedimentation zone. A charcoal sample collected 10 cm above the base of unit II4 has yielded a calibrated age at 2 sigma of 1645-1950 cal. yr. AD, with a more probable age range of 1734-1806 cal. yr. AD (53% probability) (**Table 1**).

The upper package III records episodic anthropogenic fills, including five units (III1 to III5) with markedly different colours and an exposed thickness in the trench of 2.4 m. It occurs NE of 37 m, and the units show an overall onlap arrangement and thickening towards the sinkhole centre. A bottle manufactured in the 1960s was found within unit III1. Units III1, III3 and III5 are restricted to the NE sector of the trench affected by higher subsidence related to collapse fault F2 and display upward dip attenuation; from 22º to 3º at the top of units III1 and III5, respectively. This fault offsets units III1 and III3 and is truncated by the base of unit III4.

In agreement with field observations and geophysical data, the trench reveals that the sinkhole is much larger than the depression mapped from old aerial photographs. Evidence of recent deformation in the trench indicate that the actual edge of the sinkhole, located at fault F1, is situated around 50 m to the SW of the initially mapped boundary, involving a radius increase from around 20-30 m to 70-80 m in that sector (**Fig. 3**). The structural and stratigraphic relationships observed in the trench can be attributed to sagging and collapse subsidence mechanisms, with both progressive and episodic deformation. The terrace deposit and the surficial soil (units Ia and S) have a horizontal attitude SW of fault F1. Fault F1 is a subvertical failure plane with shear fabrics and an associated system of dilated fissures in package I. It reaches the surface and offsets 15 cm the base of unit S and shows a minimum throw of 40 cm on the terrace deposit, estimated on the basis of a faulted sand bed only preserved in the downthrown block. Between fault F1 and 25 m, the terrace gravels show a very gentle apparent dip to the NE. To the NE of 25 m the terrace deposit dips 7-8º, which can be considered as a good approximation for the actual dip given the roughly radial distribution of the trench with respect to the sinkhole. Between faults F1 and F2 we have mapped seven fissures (f1 to f7), all of them with a steep outward and antithetic dip, except f4 that shows a vertical attitude and a sharp step. Some fissures are interrupted in the more competent calcic horizon developed in the upper part of the terrace deposit (f1, f3 and f4), whereas others reach the surface (f5 and f6) or penetrate

into the anthropogenic fill (f7). The fissures are expressed as dilated joints with no vertical separation and bands up to 15 cm wide of loose gravels. Their orientation, as well as that of fault F1, measured using the position of the planes on both walls of the trench, show consistent azimuths within the range N135-160E, indicating extension towards the centre of the sinkhole. These discontinuities accommodate part of the extension required to counterbalance the centripetal shortening related to sagging subsidence. The rest of the extension may be accommodated by inappreciable continuous layer-parallel dilation in the granular deposits. The cumulative wedge out that shows the natural sinkhole fill (package II), with dips ranging between 8º and 3º at 50 m, record progressive sagging subsidence (e.g., Gutiérrez et al., 2012; Carbonel et al., 2014). The NE dipping fault F2 shows a sharp over-steepening in the weaker recent deposits (pseudo-reverse fault) and the adjacent sediments in the footwall are affected by downward flexing (fault dragging). This fault offsets 15 cm unit III3 and is truncated by the base of unit III4, indicating an episode of displacement between both anthropogenic units. Fault F2 must be a secondary structure associated with a master collapse fault located to the NE.

The contribution of the two subsidence mechanisms proved in the trenched sector of the sinkhole can be estimated assuming that the terrace and the top of the units of the sinkhole fill were horizontal at their time of deposition. Collapse faulting accommodates minimum vertical displacements of 40 cm and 15 cm in faults F1 and F2, respectively. The trench does not cover the main normal fault that controls the inner collapse. Sagging, responsible for the inward tilting, is the main subsidence mechanism in the outer sector of the sinkhole. It has caused vertical displacements of 3.45 m between faults F1 and F2 and 0.7 m NE of fault F2. The cumulative subsidence in the trench reaches 4.7 m and the relative contribution of collapse and sagging are around 12% and 88%, respectively. Cumulative subsidence may be also roughly estimated at 6.3 m summing the aggregate thickness of the sinkhole deposits (4.6 m) and the elevation difference of the ground surface (1.7 m). Unfortunately, it was not possible to constrain the age of the sinkhole by dating the base of the sinkhole fill. The only available date indicates that the sinkhole is older than 1734-1806 cal. yr AD. We can estimate a minimum subsidence rate of 1.7-1.1 cm/yr at the NE end of the trench considering the thickness of the anthropogenic fill (package III, 2.4 m) and the available maximum age for those sediments. These values are in agreement with subsidence rates

measured by DInSAR (Galve et al., 2015 and referecences therein), high-precision levelling (Desir et al., 2016) and 3D laser scanner (Benito-Calvo et al., 2016) in active sinkholes in the area, and with long-term subsidence rates inferred by trenching and geochronological data (Gutiérrez et al., 2017; Carbonel et al., 2014).

*Trench T2*

This NE-SW-oriented trench was excavated across the northern margin of the depression mapped on the aerial photographs from 1956, and reached 10 m in length (**Fig. 3, 4A**). It exposed a buried collapse fault with an associated fissure and 5 sedimentary packages (I to V) bounded by marked stratigraphic discontinuities (unconformities or artificial-excavation surfaces) (**Figs. 7, 8**). The oldest package I (units Ia and Ib), equivalent to that of trench T1, is a pre-sinkhole gravelly terrace deposit. See description of sedimentary units in **Figure 8**. The terrace deposit occurs of both sides of the fault with a vertical offset of 1 m. The associated 25 cm wide fissure abuts the shear zone of the fault and is filled by loose reoriented gravel derived from the terrace. The terrace shows a gentle SW dip on the footwall, indicating that the edge of the sinkhole is somewhere to the NE of the trench. On the downthrown block the terrace deposit shows an apparent inward dip of around 15º.

Package II is interpreted as a faulted natural sinkhole fill that comprises two units (II1 and II2). Unit II2 is also offset by the fault 1 m and overlaps the fissure fill on the downthrown block. The irregular top of unit II1 in the downthrown block, where unit II2 is missing, is interpreted as an artificial excavation surface, similarly to the top of unit II2 in the footwall. Package III is also a faulted natural sinkhole fill confined to the downthrown block and bounded by artificial excavation surfaces. This package fills and seals a vertical fissure 5-10 cm wide open through the underlying packages. Unit III1 is a colluvial wedge made up of pebble gravel with the long axes of the clasts gently dipping away from the fault (**Fig. 8**). A charcoal sample collected 15 cm above its base has provided an age of 1664-1950 cal. yr. AD, with a more probable age range of 1719-1820 cal. yr. AD (50% probability), which essentially coincides with that obtained for unit II4 in trench T1 (**Table 1**).

Package IV is mostly an anthropogenic deposit consisting of three units (IV1, IV2, and IV3) that buries an excavation surface and the scarp related to the collapse fault (free face contact). This package shows a general inward dip of 18º that could correspond to its original attitude (syndepositional dip) formed in tipped material. The wedge-shaped unit IV3 that abuts the fault scarp could be interpreted as a colluvial wedge (**Fig. 8**). However, its original geometry is uncertain since its top may correspond to an artificial excavation surface. Package V is an apparently undeformed anthropogenic fill deposited across the fault scarp that rapidly thickens towards the sinkhole center reaching more than 2.2 m thick.

The stratigraphic and structural relationships observed in the trench together with the retrodeformation analysis shown in **Figure 9** allows the following sequence of deformation and depositional/erosional events to be inferred: (1) Opening of fissure on terrace surface involving downward tilting on the SW side and infill of the fissure by lose gravel. (2) Accumulation of natural sinkhole fill deposit corresponding to package II across the fissure. (3) Collapse faulting of packages I and II and partial excavation of package II in the downthrown block; the collapse fault coincides with the fissure (4) Accumulation of the colluvial wedge 0.3 m thick (lower part of package III) shed from the sinkhole scarp. (5) Deposition of the upper part of package III abutting a free face contact and deep excavation into packages III, II and I. (6) Accumulation of package IV and probable artificial levelling of the surface. (7) Rejuvenation of collapse fault. (8) Accumulation of colluvial wedge 0.30 m thick and concomitant scarp degradation. (9) Artificial accumulation of package V across the buried fault scarp.

The trench records a total vertical displacement of 2.1 m as measured on the top of unit Ib, of which 1.1 m are related to tilting in the downthrown block and 1 m to faulting. The presence of two stacked colluvial wedges, both 30 cm thick, together with the upward truncation of the fault by non-deformed deposits, indicate that the fault has experienced two discrete collapse events of around 0.5 m, accounting for the total throw of 1 m recorded in the trench. The most probable age range obtained from the lower wedge provides an approximation to the timing of the first collapse event (1719-1820 cal. yr. AD). In agreement with trench T1, this trench reveals that the sinkhole has a larger extent than that interpreted from the 1956 aerial photographs. This interpretation

is supported by the accumulation of sinkhole fill deposits on both sides of the fault and the tilting of the terrace deposits on the footwall.

## 5. Rosales sinkhole

### 5.1. Description of the site and cartographic problem

The Rosales sinkhole is located in the Rosales del Canal suburb, in the southwest sector of Zaragoza city. This doline, currently buried by man-made deposits, is spatially associated with two geomorphic units (**Fig. 10**): (1) a terrace of the Ebro River, perched around 50 m above the river channel; and (2) a flat-bottomed valley incised into the terrace deposit. The sinkhole is also associated with an irrigation ditch built along the edge of the valley, at the foot of the slope carved in the terrace deposits (**Fig. 10**). This sinkhole was initially mapped in a report that includes a cartographic inventory as an anomalous semi-circular depression 70 m in diameter restricted to the western side of the ditch (Simón et al., 1998). According to this map, the sinkhole affects the terrace, but not the younger infilled valley situated to the east of the ditch (1998 edge in **figure 11**). Subsequently, in a geotechnical report of 2004, the sinkhole was mapped as an E-W oriented ellipsoidal depression with major and minor axes of around 80 m and 60 m, respectively (2004 edge in **figure 11**). This cartographic interpretation implicitly discards the semi-circular geometry and proposes that subsidence has affected a portion of the valley east of the ditch as much as 25 m wide. This sinkhole outline together with a proposed setback distance around it widely overlapped a plot of land proposed for the construction of a multi-storey building. The mapped sinkhole has restrictive implications for urban planning. In a later geotechnical report produced in 2011, the sinkhole edge was delineated as a sub-circular area 30-35 m in diameter abutting the ditch to the west (2011 edge in **figure 11**). This new cartographic interpretation was based on the identification in aerial photographs from 1956 of a sub-circular depression nested within the semi-circular depression located west of the ditch (**Fig. 10**) and on a thorough geophysical survey. The geophysical investigation covered the sinkhole site and its vicinity and included the application of several methods: (1) magnetometry (map of residual anomalies of the magnetic field derived from spatially-dense measurements of the intensity and vertical gradient of the magnetic field); (2) multi-frequency electromagnetic field (maps of apparent electromagnetic susceptibility and conductivity); (3) ground-penetrating radar (GPR) using a 100 MHz shielded antenna.

The geophysical data did not reveal anomalies east of the ditch attributable to the presence of a sinkhole.

The buried sinkhole can be identified in old aerial photographs. The grey-scale images taken in 1956 (approximate scale 1:30,000), display a conspicuous and steep-sided semi-circular depression located west of the ditch (**Fig. 10**). This depression resembles an anomalous half-collapse-sinkhole superimposed on the indurated terrace deposits. Within this depression there was a shallow nested depression with sub-circular geometry. East of the ditch, the bottom of the valley shows a gentle inclination towards the sinkhole, which was probably functioning as a swallow hole (ponor). In the grey-scale aerial photographs of 1970 (approximate scale 1:15,000), the semi-circular depression was largely filled by anthropogenic deposits, but still recognisable (**Fig. 10**). The geomorphic expression of the depression was obliterated in the early 1990s by extensive accumulation of artificial deposits.

### 5.2. Locating the sinkhole edge by mapping and trenching

Previous investigations essentially proposed two options for the spatial distribution of the sinkhole with respect to the plot of land east of the ditch, where the construction of a building was projected (**Fig. 11**): (1) the sinkhole is restricted to the west of the ditch and does not affect the flat-bottomed infilled valley (1998 and 2011 edges); and (2) the sinkhole affects both the terrace and a 25 m wide zone within of the incised valley (2004 edge). However, the floor of the valley east of the ditch in the aerial photographs of 1956 shows an inclination towards the sinkhole (valley edge; **Fig. 10**). This geomorphic anomaly can be explained by two non-excluding interpretations: (1) the valley floor has been affected by subsidence and consequently should be considered as unstable ground; and/or (2) the gradient of the land surface is related to localised erosion by surface flows that used to drain towards the sinkhole. In order to elucidate whether dissolution-induced subsidence has affected the land east of the ditch, and establish the location of the eastern edge of the sinkhole on the basis of objective data, we produced a detailed map of the site and excavated a trench.

During the field survey we tried to find evidence of deformation on the ground surface and the ditch. the remains of the ditch showed evidence of deformation in four places,

including open cracks and conspicuous tilting of the eastern wall towards the valley attributable to lack of basal support (**Fig. 11**). This eastward tilting supported the option that active subsidence also affects the valley east of the ditch. Moreover, the damage recorded at three points was outside the edge of the sinkhole mapped in 2004 and 2011.

A trench 45 m long was excavated from the east side of the ditch towards the valley with a N45E orientation (**Fig. 11**). The excavation exposed two sedimentary packages (**Fig. 12**). The lower package was a terrace deposit consisting of reddish brown cohesive sand with scattered rounded gravels and intercalated tabular beds of sub-rounded and polymictic gravels. The upper package, corresponding to the valley fill, was composed of two beds of massive silts with different colours and proportions of floating clasts. At a distance of 35 m from the ditch, all the stratigraphic units showed a change from a subhorizontal attitude to a clear dip of 5º towards the SW (sinkhole center). Consistently, the valley fill deposits (upper package) showed an anomalous thickness increase within the same sector, changing from 0.5 m to 1.3 m in the valley margin (**Fig. 12**). One would expect to find the wedging out of the stratigraphic units of the upper package towards the valley margin. These geometrical relationships allowed us to infer the following information about the sinkhole: (1) The sinkhole edge is located east of the ditch, at a distance of 35 m along the trace of the trench. The trench provides unambiguous evidence indicating that subsidence affects a larger area that those proposed in all the previous studies based on aerial photograph interpretation, field surveys and geophysical investigations (**Fig. 11**). (2) Subsidence in the incised valley, underlain by more ductile deposits than in the terrace capped by a well-developed petrocalcic horizon, has been accommodated by sagging. (3) The dip of the sedimentary units towards the sinkhole center and the anomalous thickening of the valley fill deposits (upper package) provide a rough estimate of 0.8 m for the cumulative subsidence that occurred after the deposition of the lower package. Unfortunately, we did not find material that could be radiocarbon dated in these deformed sediments.

## 6. Ventas sinkhole

The Ventas sinkhole is a buried depression located on the lowermost terrace of the Ebro River above the floodplain, around 5 km NW of Zaragoza city. This doline, nowadays

filled by anthropogenic deposits, is situated on the northeastern side and beneath the A-68 highway, in a plot of land susceptible for industrial development (**Fig. 13**). The previously existing depression was recognised in a detailed topographic map from 1969 produced at a scale of 1:2000 with contour interval of 1 m (cartographic data of Zaragoza Municipality). In this map the depression is depicted with a dashed contour as a semicircular basin around 50 m across adjacent to the NE side of the old A-68 road. Nowadays, the site shows a flat topography and the overlying human-built structure does not show any evidence of deformation attributable to sinkhole-related subsidence (**Fig. 13**).

Three trenches (T1, T2 and T3) with a radial distribution were excavated in order to: (1) elucidate whether the buried depression depicted in the old map corresponds to an artificial excavation or an infilled sinkhole; and (2) determine, in the latter case, the edges and characteristics of the sinkhole. Trench T3, 35 m long, exposed three units in ascending order (**Fig. 13**): (1) a massive terrace deposit; (2) a natural sinkhole fill; and (3) an anthropogenic fill. From the vertical reference line 16 units 1 and 2 showed a clear dip of 4-6º to the SW. The top of unit 1 shows a vertical displacement within the trench of 0.8 m. Moreover, the anthropogenic fill shows a thickness increase from 0.5 m at reference line 16 to 1.3 m in the SW edge of the trench. Between 20 and 23 m the more brittle calcic horizon developed on the terrace deposit displayed a horizontal crack 30 cm long and 3 cm wide, and a zone 0.7 m thick with an irregular base in which the terrace gravels were loose and dilated, with the intergranular spaces filled by reddish fines derived from the overlying unit. This evidence of deformation may be related to local extension caused by the flexure of the partially indurated alluvium. Trench T1, 31 m long, was excavated to the W of trench T3 and parallel to the A-68 highway. This trench showed a similar stratigraphy and structure to that found in trench T3. The edge of the sinkhole, indicated in **figure 13**, was established on the basis of the following evidence: (1) change in the attitude of the terrace gravels from horizontal to a dip of 3º towards the inner part of the sinkhole (SE), with a vertical displacement of 0.8 m; (2) the natural sinkhole fill pinching out at that point and thickening concordantly with the dip of the underlying unit; and (3) thickening of the anthropogenic fill. Similar criteria were also used to determine the edge of the sinkhole in trench T2. In this case the terrace gravels showed an apparent dip of 3º to the WNW.

The integration of the stratigraphic and structural relationships observed in the three trenches allowed us to infer the following observations about the buried depression: (1) it clearly corresponds to a subsidence sinkhole; (2) the overall subsidence structure corresponds to a structural basin with centripetal dips (sagging sinkhole) and a minimum cumulative subsidence of 0.8 m; (3) the edges of the sinkhole, around 55 m across, can be defined with a high level of confidence on the NE side of the A-68 highway; (4) the buried sinkhole is partially located beneath the A-68 highway. The absence of deformation evidence in the A-68 highway, built decades ago, strongly suggests that it is an inactive sinkhole.

## 7. Discussion

The trenching investigations presented in this work illustrate that the actual extent of the areas affected by subsidence may be much larger than those inferred by geomorphic mapping and geophysical surveys and thus require careful evaluation. They also demonstrate that trenching can be a very effective method for locating accurately and unambiguously the edge of the subsidence areas affected by ground displacement.

The trenches excavated in the airport-road sinkhole reveal that it corresponds to a complex sagging and collapse structure. It comprises an inner collapse that had conspicuous geomorphic expression before its anthropogenic filling, and a broad marginal zone affected by downward bending and fissuring, not recognisable from aerial photograph interpretation and field surveying (**Figs. 3, 4B**). The trench showed that the affected area needed to be expanded by three times the radius of the sinkhole mapped on the basis of geomorphic criteria, from 25 m to 75 m (**Fig. 3**). This involves a subsidence-affected area that is 7 times larger than initially identified, increasing from around 2,800 $m^2$ to 20,000 $m^2$. The buried sinkhole was clearly captured by GPR and ERI, but these indirect techniques did not provide precise information on the location of the edges of the subsidence area (**Fig. 5**).

In the case of the Rosales sinkhole, there were three highly different cartographic alternatives previously proposed. The most recent one, largely based on a thorough previous geophysical investigation conducted for a geotechnical report, suggested a

spatially restricted collapse sinkhole with a radius of around 17 m. However, the trench investigated in the buried sector of the sinkhole, together with detailed surface mapping, revealed a much larger sinkhole with a radius of around 42 m (Fig. 13). This more realistic sinkhole map involves a sixfold increase in the sinkhole area, from 900 $m^2$ to 5500 $m^2$, with implications for land-use planning at this site. In the trench excavated in the Rosales sinkhole, the edge of the subsidence area was identified by a change from horizontal to dipping strata in the pre-sinkhole deposits and anomalous tilting and thickening of valley-fill deposits towards the margin of the valley.

The buried Ventas sinkhole was investigated through three radial trenches (**Fig. 13**). The integration of the data gathered from the trenches allowed us to confirm that the depression mapped from old topographic maps was not an anthropogenic feature, but a shallow sagging sinkhole with basin structure, as defined by centripetal dips. The trenches were used to precisely locate the boundary of the subsidence area at three points and map the edge by interpolation. Here, the limit of the area affected by subsidence was also identified by a change in the attitude of the pre-sinkhole sediments, from horizontal to dipping, and thickenings or pinch outs in the sinkhole-fill deposits.

The presented work shows that site investigations that utilise trenching may provide very different and more realistic results on the edges of the subsidence areas than those obtained by other conventional methods such as geomorphic mapping and shallow geophysics. In the airport-road and Rosales sinkholes, trenches reveal that the subsidence areas associated with those dolines are around 6-7 times larger than the ones proposed in previous maps. In contrast, a trenching investigation conducted in a large sagging sinkhole in the evaporite karst of the Fluvia Valley, NE Spain, revealed that the radius of the area affected by subsidence was around 60 m smaller than that of the topographic depression. In this latter case, natural and anthropogenic erosion at the sinkhole margin resulted in a significant expansion of the depression (Fabregat et al., 2017). Consequently, the data gathered by the underutilized trenching technique may have beneficial societal and economic implications for the following reasons: (1) it allows sinkhole edges to be more accurately mapped and more effective preventive measures to be applied; and (2) it may help to reduce setback distances by minimizing the uncertainties associated with the location of the subsidence areas.

Comprehensive trenching investigations are time consuming and require the participation of experienced professionals. However, if the objective is locating the edges of the subsidence area, this can be achieved quite quickly and with a high level of confidence by digging radial trenches, cleaning the walls, and focusing the survey on the location of the boundary between the deformed and non-deformed sediments, without carrying out detailed logging and retrodeformation analyses. This rarely used but efficient technique is particularly useful in evaporite karst areas, where the sagging mechanism plays an important role in the development of sinkholes (e.g., Gutiérrez et al., 2008a). Subsidence related to this passive bending mechanism may be difficult to perceive due to its geomorphic expression, but may lead to differential settlement and severe damage to human structures (**Fig. 14**).

As shown in previous investigations carried out in Spain (Carbonel et al., 2014; Fabregat et al., 2017; Gutiérrez et al., 2017 and references therein) and in Saudi Arabia (Youssef et al., 2016), the trenching technique provides abundant objective information on the characteristics and past behaviour of sinkholes. It also incorporates a temporal dimension (numerical ages, geometrical relationships) generally lacking in other investigation methods (boreholes, geophysics). These data significantly contribute to develop the basis for reliable hazard assessments and predictions. The deformation style and the stratigraphic and structural relationships provide information about the subsidence mechanisms and the kinematic style. In the complex airport sinkhole, collapse faulting is the dominant process in the inner zone, whereas sagging accompanied by extensional fissuring prevail in the outer zone. Collapse faulting is mainly an episodic process as indicated by the presence of colluvial wedges and upward fault truncations (**Figs. 7, 8, 9**). Conversely, sagging is most probably a gradual process as suggested by the cumulative wedge outs observed in the sinkhole fill deposits (**Fig. 6**). Geometrical relationships observed in the Ventas sinkhole and the trenched sector of the Rosales sinkhole point to progressive subsidence (bed thickenings and upward dip attenuation in the sinkhole fill). The relative chronology inferred on the basis of structural and stratigraphic relationships may also provide some information on the spatial-temporal evolution of sinkholes (expanding versus contracting). For instance, the onlap arrangement of the sinkhole fill deposits observed in trench T1 of the airport-road sinkhole indicate an expansion of the accumulation zone of 16 m. Structural and stratigraphic measurements may be used to assess the contribution of different

structures and subsidence mechanisms to the overall deformation. These are frequently minimum values restricted by the orientation of the trench with respect to the structures, (if not perpendicular to the structures), and the limited depth and length of the excavations (e.g. Carbonel et al., 2014; Sevil et al., 2017). Trenches also offer the possibility of collecting direct samples for the application of geochronological methods. Dating provides information on the age of the sinkholes and subsidence events and can be used to estimate long-term subsidence rates. Although this was not a priority in the examples presented in this work, calibrated radiocarbon ages from the airport-road sinkholes allowed us to calculate minimum subsidence rates for the marginal sagging zone as large as 1.7-1.1 cm/yr.

The literature on setback distances from sinkholes is scarce and the values recommended from different investigations are highly dissimilar and generally not justified. Zhou and Beck (2008) reported that in Monroe County, Indiana, the setback for the construction of residential and commercial buildings is established at 7.6 m for sinkholes smaller than 0.1 ha. For sinkholes larger than 0.1 ha, the setback should be 15 m from the post-development sinkhole flooding area or 7.6 m from the rim of the sinkhole, whichever is less. In Knox County and the town of Farragut, of Tennessee, a 15 m setback was recommended. Kemmerly (1993), in his planning model for sinkhole hazards, proposed a setback of 152 m (500 feet) from sinkhole edges where development should be restricted. The Virginia State guidelines for karst assessments indicated a minimum buffer of 30 m (100 feet) around the boundaries of the inventoried dolines (Virginia Cave Board, 2017). The karst mitigation plan for the Atlantic Coast Pipeline project, a gas pipeline that will traverse around 52 km of karst terrain in West Virginia and North Carolina, recommended a setback of 91 m (300 feet) from sinkholes where land disturbances should be avoided (GeoConcepts Engineering, 2015). Fleury (2009) presents a table including no-build setback values used by municipalities in the USA, ranging from 6 to 30 m (20-100 feet). Setbacks to prevent aquifer contamination may reach up to 152 m (500 feet). He also mentioned that setbacks are often under heavy political pressure from developers or property owners who seek waivers or exemptions from standoff requirement.

In the Zaragoza municipality, where sinkhole damage to buildings is relatively frequent, the setback is established specifically for each sinkhole (Gerencia de Urbanismo, pers.

comm.). Nonetheless, a sinkhole inventory incorporated in the land-use planning of the city propose a buffer zone of 15 m around every sinkhole to account for the uncertainties associated with the location of the sinkhole edges and the potential occurrence of small collapses in the marginal zones (Simón et al., 1998). However, the results of our investigation show that a setback of 15 m may be clearly insufficient and lead to unsafe planning. Trenches indicate that the actual radii of the airport-road and the Rosales sinkholes are around 50 m and 25 m larger than those indicated in previous maps (**Figs. 3, 11**). For urban planning, it would be advisable to define the standoff zones associated with existing sinkholes following a phased approach. In a first phase, the edges of the subsidence areas should be mapped accurately, preferably incorporating data from trenches. The application of this technique may lead to significant changes in the cartographic inventories, but minimizes the mapping uncertainties. In a subsequent phase, a setback should be established. In our opinion, it would be preferable to establish and justify a setback distance for each sinkhole or sinkhole area considering a number of factors: (1) The precision versus the uncertainty of the mapped boundaries. Subsidence areas mapped with a high level of accuracy may allow the reduction of the setback. As indicated above, this uncertainty about the sinkhole boundaries may be reduced by applying the trenching technique. (2) Sinkhole type and subsidence mechanisms. For instance, sagging sinkholes tend to produce depressions and subsidence structures with poorly-defined edges (**Fig. 14**). (3) Sinkhole depth and susceptibility of the sinkhole edges to retreat by slope failures and gullying. Cover collapses, even those with limited depth, may enlarge rapidly by mass wasting and erosion processes when the margins are underlain by weak and erodible deposits (**Fig. 15**). (4) Degree of activity of the sinkhole. The future expansion of the subsidence area in active sinkholes is more likely than in inactive sinkholes. (5) Short- and long-term evolution of the sinkhole. Some sinkholes may show evidence of recent growth (e.g. Carbonel et al., 2014), whereas others may display a trend whereby subsidence affects progressively more restricted areas (e.g., nested sinkholes in older depressions; Sevil et al., 2017). (6) Clustering versus scattering of the sinkholes and tendency of the new subsidence events to occur in the vicinity of pre-existing sinkholes (Kemmerly, 1982). This spatial-temporal pattern can be explored through the nearest neighbour analysis (Williams, 1972; Gutiérrez, 2016 and references therein) and constructing cumulative frequency curves with the distances to the nearest neighbour (e.g., Fabregat et al., 2017). (7) The characteristics of the engineering structure, considering factors such as

its function, foundation type, influence on the local hydrology or the load imposed on the ground.

The concepts and approaches discussed in this paper about the application of the trenching technique and the establishment of setback distances could be partially transferred to the investigation and management of other hazardous processes that involve the deformation of the ground such as landslides, earth fissures, gravitational surface faulting, or subsidence related to cryokarst (thawing of ground ice).

**8. Conclusions**

- The actual extent of the unstable areas affected by subsidence in sinkholes may be much larger than that inferred by surface mapping and geophysical surveys. This deviation may be particularly large in sagging sinkholes, in which subtle downward bending at the margins may produce unrecognisable geomorphic expression.
- Trenching allows locating precisely the edges of the subsidence areas. Eliminating the uncertainty associated with sinkhole mapping via trenching, may allow reducing significantly the setback distance, with the consequent beneficial economic implications.
- No-build setback distances should be established considering the specific characteristics of each sinkhole and its setting, rather than recommending an arbitrary and general standoff value.
- The set-back distance recommend by land-use planners, typically around 15 m, may be insufficient due to imprecise mapping of the subsidence area and the potential expansion of sinkhole depressions by subsidence, slope failures and gullying.
- The trenching technique provides abundant objective information on the characteristics and past behaviour of sinkholes, incorporating a temporal dimension generally lacking in other common investigation methods (boreholes, geophysics). These data, covering a broader temporal range than the instrumental and historical records, may be used as the basis for reliable hazard assessment and effective risk mitigation.

**Acknowledgements**

This work has been funded by project CGL2013-40867-P (Ministerio de Economía y Competitividad, Spain). Mario Zarroca has a Serra Húnter fellowship at the Universidad Autónoma de Barcelona.

**References**

Acero, P., Auqué, L., Galve, J.P., Gutiérrez, F., Carbonel, D., Gimeno, M.J., Yechieli, Y., Asta, M.P., Gómez, J.B., 2015. Evaluation of geochemical and hydrogeological processes by geochemical modelling in an area affected by evaporite karstification. Journal of Hydrology 529, 1874-1889.

Benito-Calvo, A., Gutiérrez, F., Carbonel, D., Desir, G., Guerrero, J., Magri, O., Karampaglidis, T., Fabregat, I., 2016. Measuring deformation related to active sinkholes with ground-based 3D laser scanner. A case study in the evaporite karst of the Ebro Valley, NE Spain. In: Durán, J.J., Montes, M., Robador, A., Salazar, A. (eds.). Comprendiendo el relieve: Del pasado al futuro. XIV Reunión Nacional de Geomorfología, Málaga, pp. 599-606.

Boncio, P., Galli, P., Naso, G., Pizzi, A., 2012. Zoning Surface ruptura hazard along normal faults. Insight from the 2009 $M_w$ 6.3 L'Aquila, central Italy, earthquake and other global earthquakes. Bulletin of the Seismological Society of America 102, 918-935.

Bryant, W.A., 2010. History of the Alquist-Priorlo Earthquake Fault Zoning Act, California, USA. Environmental Engineering Geoscience 16, 7-18.

Carbonel, D., Rodríguez, V., Gutiérrez, F., McCalpin, J.P., Linares, R., Roqué, C., Zarroca, M., Guerrero, J., Sasowsky, I., 2014. Evaluation of trenching, ground penetrating radar (GPR) and electrical resistivity tomography (ERT) for sinkhole characterization. Earth Surface Processes and Landforms 39, 214-227.

Dahlin, T., Zhou, B., 2004. A numerical comparison of 2D resistivity imaging with 10 electrode arrays. Geophysical Prospecting 52, 379–398.

Desir, G., Guerrero, J., Gutiérrez, F., Carbonel, D., Merino, J., Benito, A., Fabregat, I., Roqué, C., Zarroca, M., Linares, R., 2016. Monitorización de dolinas activas en el entorno de Zaragoza mediante nivelación geométrica de alta precisión. In: Durán, J.J., Montes, M., Robador, A., Salazar, A. (eds.). Comprendiendo el relieve: Del pasado al futuro. XIV Reunión Nacional de Geomorfología, Málaga, pp. 607-613.

Fabregat, I., Gutiérrez, F., Roqué, C., Comas, X., Zarroca, M., Carbonel, D., Guerrero, J., Linares, R., 2017. Reconstructing the internal structure and long-term evolution of hazardous sinkholes combining trenching, electrical resistivity imaging (ERI) and ground penetrating radar (GPR). Geomorphology 285, 287-304.

Farrant, A.R., Cooper, A.H., 2008. Karst geohazards in the UK: the use of digital data for hazard management. Quarterly Journal of Engineering Geology and Hydrogeology 41, 339-356.

Fleury, S., 2009. Land Use Policy and Practice on Karst Terrains. Springer, 187 p.

Galve, J.P., Gutiérrez, F., Lucha, P., Bonachea, J., Cendrero, A., Gimeno, M.J., Gutiérrez, M., Pardo, G., Remondo, J., Sánchez, J.A., 2009. Sinkholes in the salt-bearing evaporite karst of the Ebro River valley upstream of Zaragoza city (NE Spain). Geomorphological mapping and analysis as a basis for risk management. Geomorphology 108, 145-158.

Galve, J.P., Castañeda, C., Gutiérrez, F., Herrera, G., 2015a. Assessing sinkhole activity in the Ebro Valley mantled evaporite karst using advanced DInSAR. Geomorphology 229, 30-44.

GeoConcepts Engineering, 2015. Karst terrain assessment, construction, monitoring and mitigation plan. Atlantic Coat Pipeline and Dominion Transmission, 17 p. http://deq.state.va.us/Portals/0/DEQ/Water/Pipelines/ACP_DomResponse401WQCResponse.pdf

Gibb, J.G., 1995. Assessment of coastal hazard zones for Northern Poverty Bay and Wainui Beach, Gisborne District. Report prepared for Gisborne District Council, 57 p. file:///C:/Users/pcp1/Downloads/CHA-Nth.-Poverty-Bay-Wainui-CHA-1995-n113147.pdf

Guerrero, J., Gutiérrez, F., Galve, J.P., 2013. Large depressions, thickened terraces, and gravitational deformation in the Ebro River valley (Zaragoza area, NE Spain): Evidence of glauberite and halite interstratal karstification. Geomorphology 196, 162-176.

Gutiérrez, F., 2016. Sinkhole hazards. Oxford Research Encyclopedia of Natural Hazard Science. Oxford University Press, pp. 1-92.

Gutiérrez, F., Guerrero, J., Lucha, P., 2008a. A genetic classification of sinkholes illustrated from evaporite paleokarst exposures in Spain. Environmental Geology 53, 993-1006.

Gutiérrez, F., Calaforra, J.M., Cardona, F., Ortí, F., Durán, J.J., Garay, P., 2008b. Geological and environmental implications of evaporite karst in Spain. Environmental Geology 53, 951-965.

Gutiérrez, F., Parise, M., De Waele, J., Jourde, H., 2014. A review on natural and human-induced geohazards and impacts in karst. Earth Science Reviews 138, 61-88.

Gutiérrez, F., Mozafari, M., Carbonel, D., Gómez, R., Raeisi, E., 2015. Leakage problems in dams built on evaporites. The case of La Loteta Dam (NE Spain), a reservoir in a large karstic depression generated by interstratal salt dissolution. Engineering Geology 185, 139-154.

Gutiérrez, F., Zarroca, M., Castañeda, C., Carbonel, D., Guerrero, J., Linares, R., Roqué, C., Lucha, P., 2017. Paleoflood records from sinkholes using an example from the Ebro River floodplain, northeastern Spain. Quaternary Research 88, 71-88.

Kemmerly, P.R., 1982. Spatial analysis of a karst depression population: Clues to genesis. Geological Society of America Bulletin 93, 1078-1086.

Kemmerly, P.R., 1993. Sinkhole hazards and risk assessment in a planning cotext. Journal of the American Planning Association 59, 221-229.

Larsen, E.W., Girvetz, E.H., Freimer, A.K., 2006. Assessing the effects of alternative setback channel constraint scenarios employing a river meander migration model. Environmental Management 37, 880-897.

Loke, M.H., Barker, R.D., 1996. Rapid least-squares inversion of apparent resistivity pseudosections by a quasi-Newton method. Geophysical Prospecting 44, 131-152

McCalpin, J.M., 1987. Recommended setback distances from active normal faults. In: Proceedings of the 23rd Symposium on Engineering Geology and Soils Engineering, Logan, Utah, pp. 35-36.

Paukstys, B., Cooper, A.H., Arustiene, J., 1999. Planning for gypsum geohazard in Lithuania and England. Engineering Geology 52, 93-103.

Pueyo-Anchuela, O., Pcoví Juan, A., Casas-Sainz, A.M., Ansón-López, D., Gil-Garbi, H., 2013. Actual extension of sinkholes: Considerations about geophysical, geomorphological, and field inspection techniques in urban planning projects in the Ebro basin (NE Spain). Geomorphology 189, 135-149.

Reimer, P.J., Bard, E., Bayliss, A., Beck, J.W., Blackwell, P.G., Bronk Ramsey, C., Grootes, P.M., Guilderson, T.P., Haflidason, H., Hajdas, I., HattŽ, C., Heaton, T.J., Hoffmann, D.L., Hogg, A.G., Hughen, K.A., Kaiser, K.F., Kromer, B., Manning, S.W., Niu, M., Reimer, R.W., Richards, D.A., Scott, E.M., Southon, J.R., Staff, R.A., Turney, C.S.M., van der Plicht, J., 2013. IntCal13 and Marine13 radiocarbon age calibration curves 0-50,000 years cal BP. Radiocarbon 55, pp. 1869–1887.

Salvany, J. M., García-Veigas, J., Ortí, F., 2007. Glauberite-halite association of the Zaragoza Gypsum Formation (Lower Miocene, Ebro Basin, NE Spain). Sedimentology 54, 443–467.

Sevil, J., Gutiérrez, F., Zarroca, M., Desir, G., Carbonel, D., Guerrero, J., Linares, R., Roqué, C., Fabregat, I., 2017. Sinkhole investigation in an urban area by trenching in combination with GPR, ERT and high-precision leveling. Mantled evaporite karst of Zaragoza city, NE Spain. Engineering Geology, submitted.

Simón, J.L., Martínez–Gil, J., Soriano, M.A., Arlegui, L., Caballero, J., 1998. Estudio de riesgos naturales en los terrenos de la orla sudoeste de suelo urbanizable. Unpublished report. https://www.zaragoza.es/contenidos/urbanismo/pgouz/memoria/anejos/anejo03/anejo031.pdf

Smith, B.H., 1994. Coastal setback and the impact of water amenities. Geographical Analysis, 26, 364-369.

Virginia Cave Board, 2017. Karst assessment standard practice. Virginia Department of Environmental Quality, 9 p. http://www.aijiuyujia.com/karst-geology-in-virginia.pdf#

Waltham, T., Bell, F., Culshaw, M., 2005. Sinkholes and subsidence. Springer, Chichester, 382 pp.

Williams, P., 1972. Morphometric analysis of polygonal karst in New Guinea. Geological Society of American Bulletin 83, 761-796.

Youssef, A.H., Al-Harbi, H.M., Gutiérrez, F., Zabramwi, Y.A., Bulkhi, A.B., Zahrani, S.A., Bahamil, A.M., Zaharani, A.J., Otaibi, Z.A., El-Haddad, B.A., 2016. Natural and human-induced sinkhole hazards in Saudi Arabia: distribution, investigation, causes and impacts. Hydrogeology Journal 24, 625-644.

Zarroca, M., Comas, X., Gutiérrez, F., Carbonel, D., Linares, R., Roqué, C., Mozafari, M., Guerrero, J., Pellicer, X.M. 2017. The application of GPR and ERI in combination with exposure logging and retrodeformation analysis to characterize sinkholes and reconstruct their impact on fluvial sedimentation. Earth Surface Processes and Landforms 42, 1049–1064.

Zhou, Q., Xu, X.,Yu, G., Chen, X., He, H., Yin, G., 2010. Width distribution of the surface ruptures associated with the Wenchuan earthquake: Implication for the setback zone of the seismogenic faults in postquake reconstruction. Bulletin of the Seismological Society of America 100, 2660-2668.

Zhou, W., Beck, B.F., 2008. Management and mitigation of sinkholes on karst lands: an overview of practical applications. Environmental Geology 55, 837-851.

**Figure captions**

Figure 1. Sketches illustrating sinkholes in which the topographic depression may be significantly larger (A) or apparently smaller (B) than the unstable area affected by ground deformation.

Figure 2. Geographic location of the investigated sinkholes in the mantled evaporate karst of the Ebro River valley, NE Spain. The Ventas and Airport-road sinkholes are located next and beneath the N-232 and N-125 roads. The Rosales sinkhole is situated in an area under urbanization in the SW sector of Zaragoza city (Images from the Instituto Geográfico Nacional).

Figure 3. Map of the airport-road sinkhole area showing the edges of the buried depression identified in orthorectified aerial photographs from 1956, direct and indirect evidence of ground subsidence, and the investigation layout, including an ERI section, the GPR profile presented in this work, and two trenches carried out along the same line for direct comparison. The map also shows the edge of the underlying subsidence structure inferred by the different methods.

Figure 4. Sinkhole depression identified in an aerial photograph taken in 1956. The edges of the buried funnel-shaped depression are depicted in figure 2.

Figure 5. A: Image taken from the N-125 road illustrating the distribution of the NE-SW oriented trenches. B: General view of trench T1 showing the general NE dip of the different sedimentary packages (I: terrace deposit; II: natural sinkhole fill; III: anthropogenic fill) and fault F2 in the NE sector of the trench.

Figure 6. Geophysical sections. (a) GPR profile and (b) ERI section acquired in the airport-road sinkhole site along the same line and coinciding with the location of the trenches (see figure 2 for location). (c) Interpretation of the ERI section.

Figure 7. Log of trench T1 and structural sketch of the trench. The numerical age corresponds to a calibrated age range with a probability of 0.53.

Figure 8. Log of trench T2. The numerical age corresponds to a calibrated age range with a probability of 0.50.

Figure 9. Image of trench T2 showing the boundaries of the sedimentary packages the colluvial wedges (CW) associated with the collapse fault.

Figure 10. Retrodeformation sequence inferred from trench T2, showing two collapse events and multiple phases of accumulation (natural and anthropogenic) and artificial excavation. See additional explanation in the text.

Figure 11. Orthorectified aerial photographs from 1956 and 1970 showing the Rosales sinkhole. The image of 1956 shows a semi-circular depression west of the ditch (terrace), with a nested subcircular collapse sinkhole, and a local anomalous gradient towards the sinkhole in the incised valley located to the east of the ditch. In the image of 1970 the semi-circular depression is largely filled but still recognizable.

Figure 12. Sketch of the Rosales sinkhole site showing the damage observed in the ditch, the location of the trench, the edges mapped in different reports and the eastern edge inferred by trenching in this work. The inset image shows the trench excavated in the infilled valley (camera looking to the SW). The terrace and the infilled valley are shown with green and yellow pattern, respectively.

Figure 13. Image of the SW sector of the trench showing the tilting of the two sedimentary packages and the thickening of the upper package towards the valley margin and the sinkhole center (I: terrace deposits; II: valley fill).

Figure 14. Figures illustrating the investigation of the Ventas sinkhole. Bottom-left: Distribution of the three trenches with radial distribution excavated on the NE side of the A-68 highway. The persons, marked with arrows, indicate the position of the edge of the sinkhole identified in the trenches. Top: Log of trench T3 (see explanation in text). Bottom-right: Image of trench T3 showing the tilting of units 1 and 2 and the thickening of unit 3 towards the SW.

Figure 15. Sagging and collapse paleosinkholes exposed in the cuttings of the Madrid-Barcelona high-speed railway in the Ebro Valley close to Zaragoza city. These sinkholes show in cross-section a synformal structure (wide arrows) with a collapse in the core (thin arrows). The master collapse faults are typically well-expressed in the surface as scarps, whereas the marginal zone affected by downward bending may be difficult to identify by surface mapping and geophysical surveys, leading to underestimated sinkhole maps. A) Subsidence affects the evaporitic bedrock and the overlying Quaternary pediment cover. B) Subsidence affects the evaporitic bedrock, which has been brecciated and partially transformed into a karstic residue in the inner collapse.

Figure 16. Examples of sinkholes affected by rapid expansion due to erosion and landsliding at their margins. A) Collapse sinkhole related to gypsum dissolution in Western Ukraine (48°45'52.15''N 25°57'57.86''E). The soft fine-grained sediments overlying the Miocene gypsum unit are affected by landslides that cause the growth and shallowing of the depression. B). Cover collapse sinkhole related to salt dissolution in the in the Jordanian coast of the Dead Sea (Al Mazraa area). Retrogressive slumps (rotational slides) of lacustrine muds at the scarped margins result in a dramatic increase of the sinkhole size. Arrow marks the position of the original edge of the sinkhole. Note the irregular topography related to the multiple backtilted slid blocks. C) Cover collapse sinkhole in a pivot-irrigation plot west of Jauf, Saudi Arabia (29°46'42.96''N 38°27'36.97''E). The edge of the sinkhole, made up of sand overlain by a gravel package, is affected by gullying. Note the earthen berm built around 15 m away for the sinkhole edge that is locally undermined by the headward expansion of a gully head.

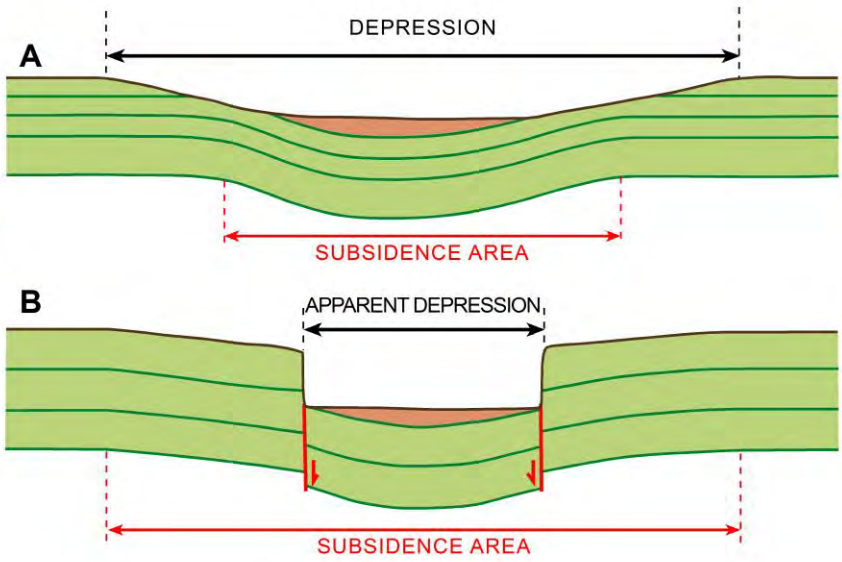


Fig. 1


Fig. 2

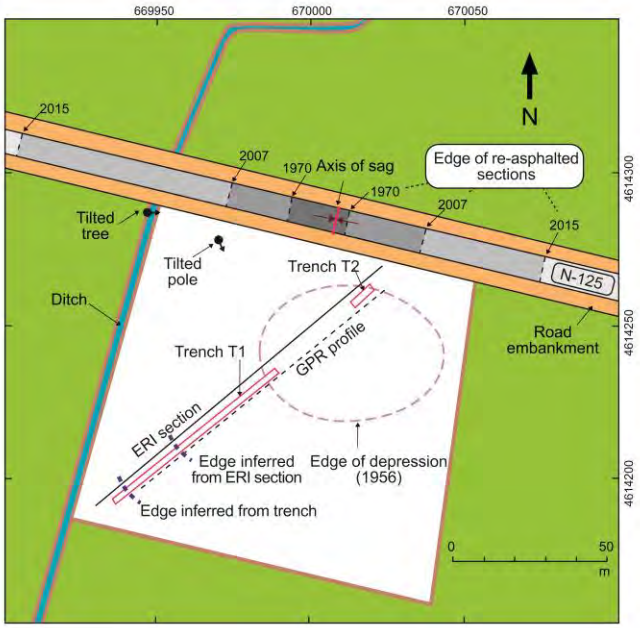


Fig. 3

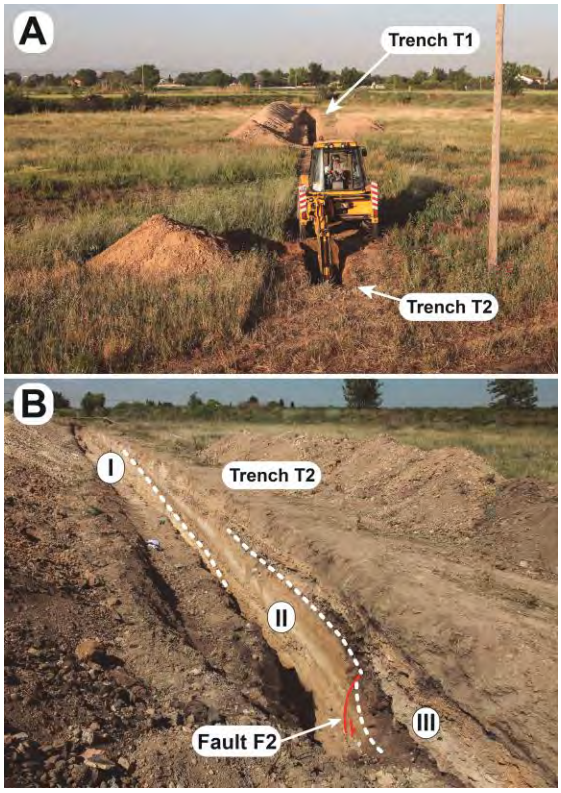


Fig. 4

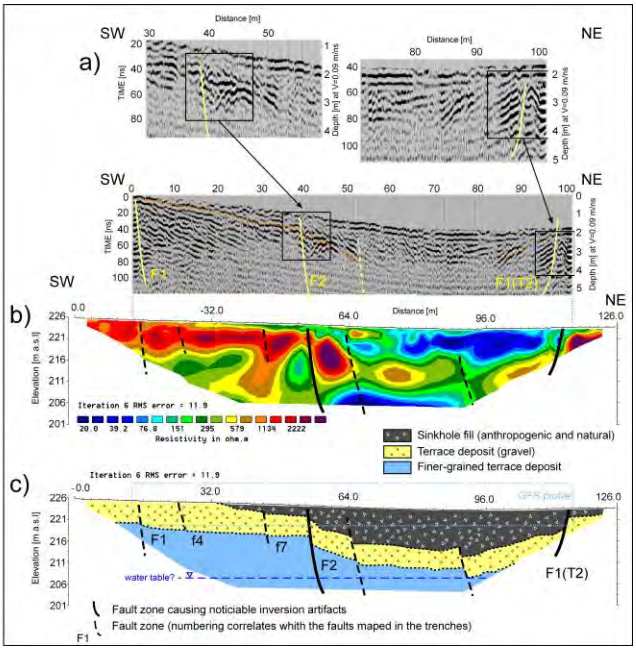


Fig. 5

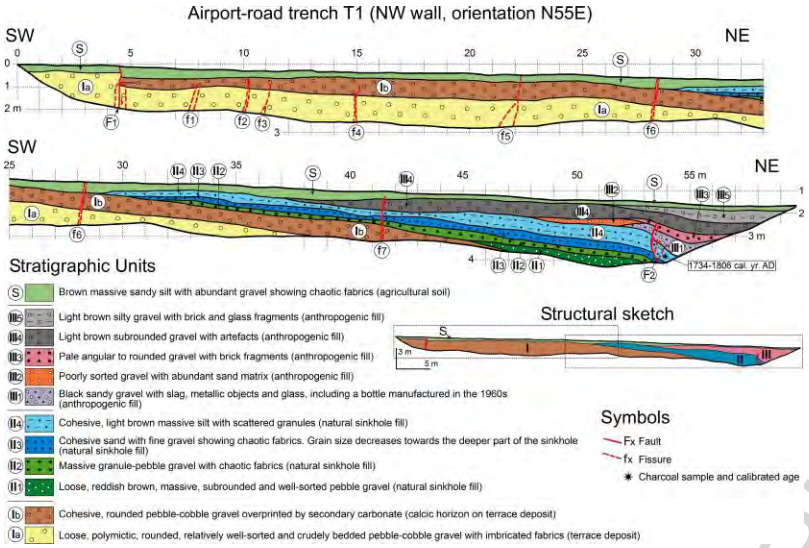


Fig. 6

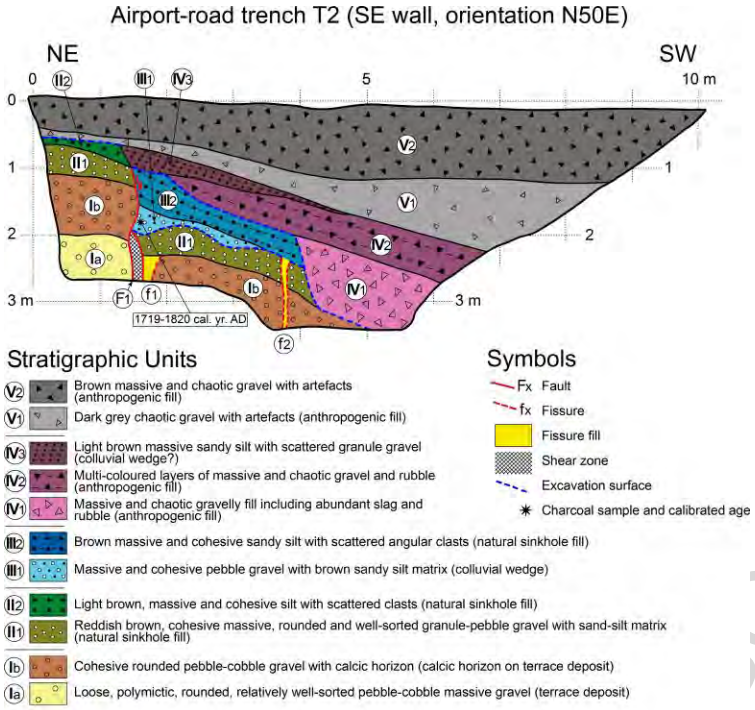


Fig. 7

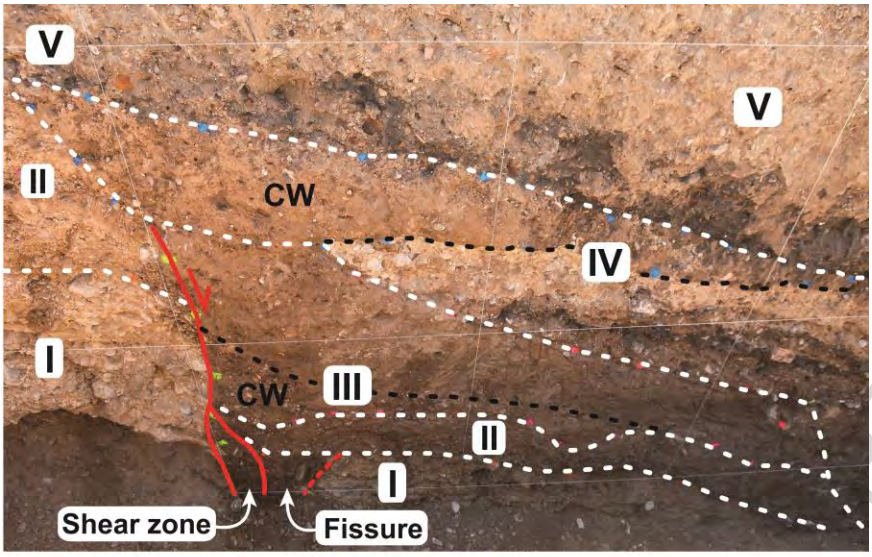


Fig. 8

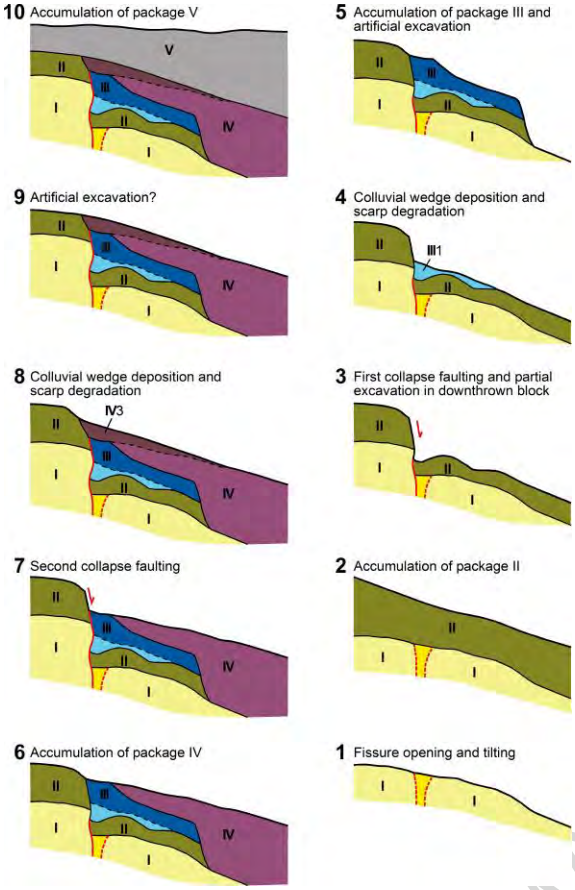


Fig. 9

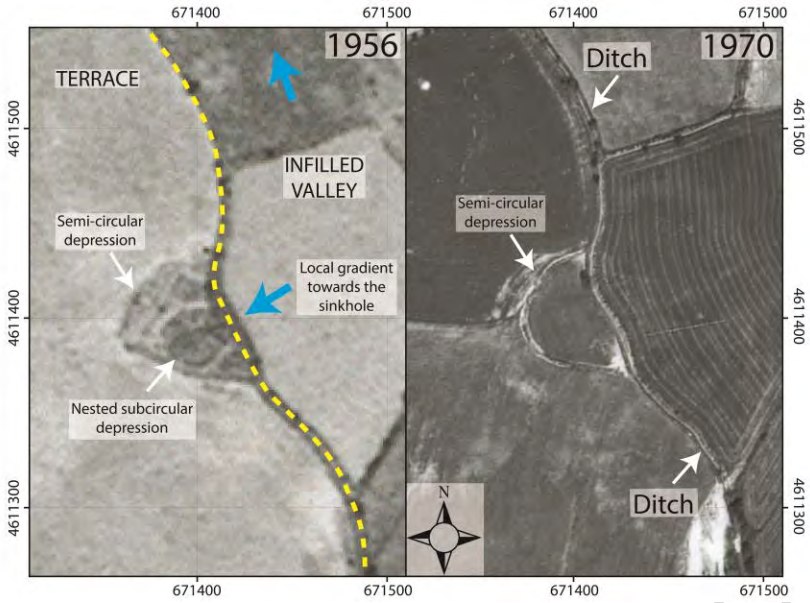


Fig. 10

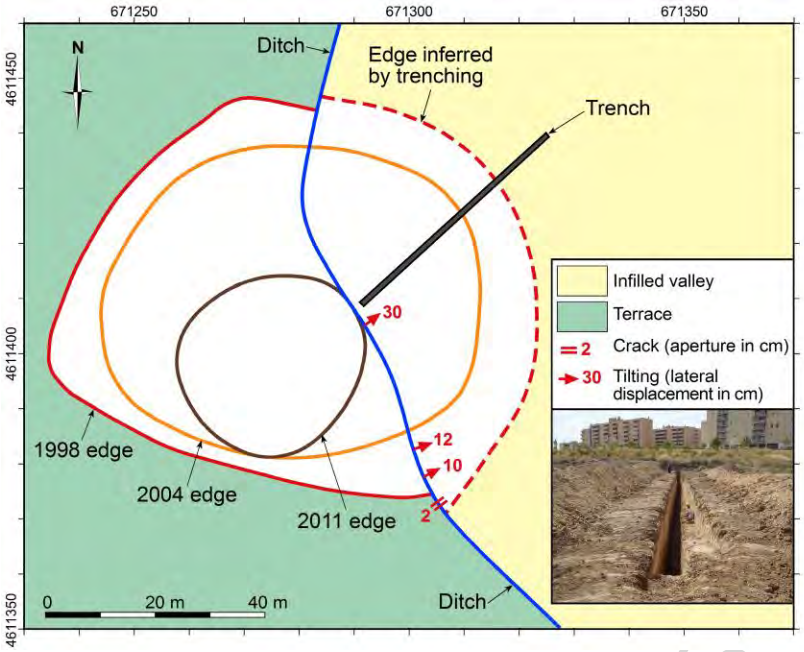


Fig. 11

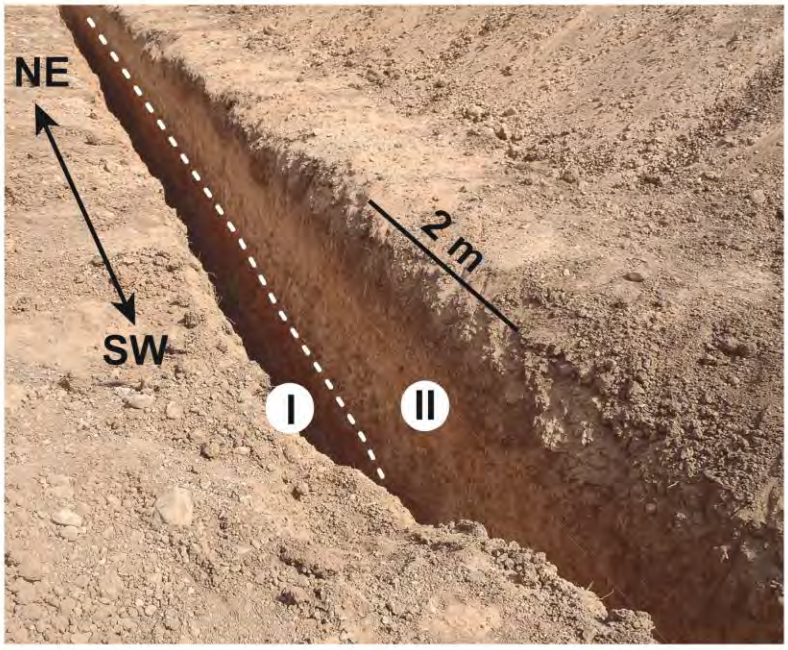


Fig. 12

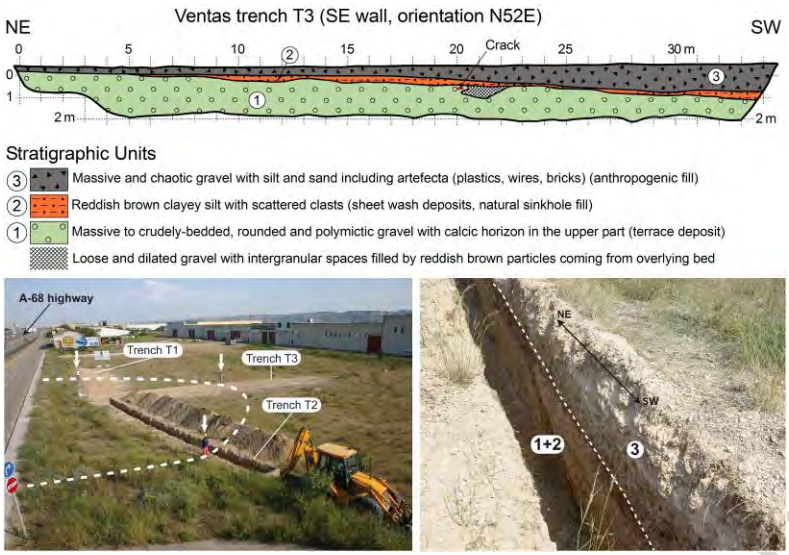


Fig. 13

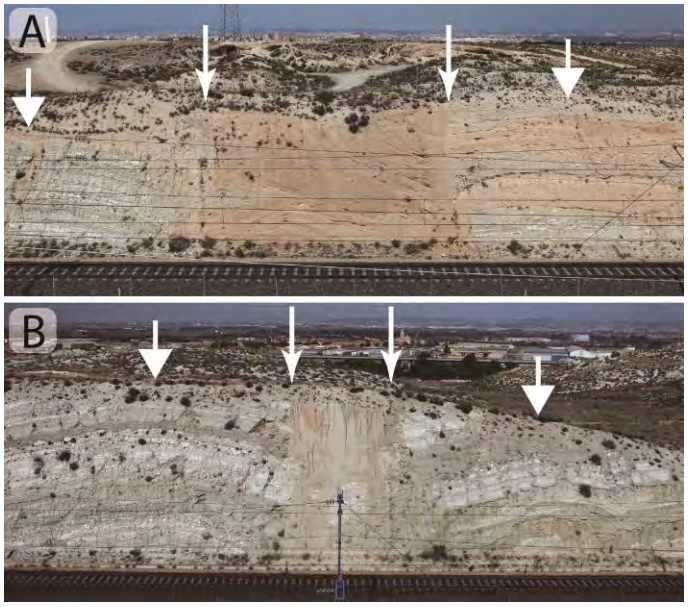


Fig. 14

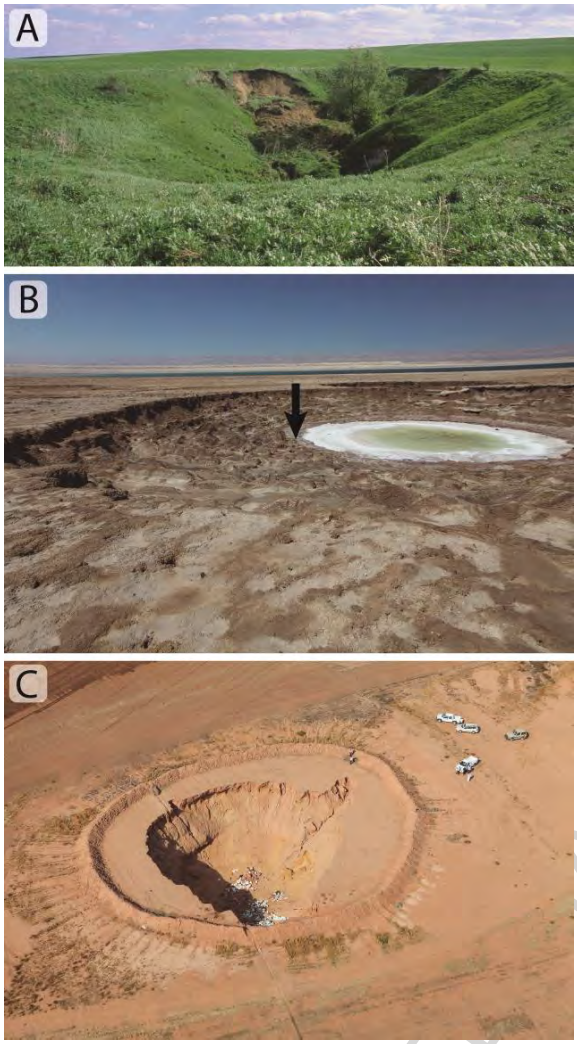


Fig. 15

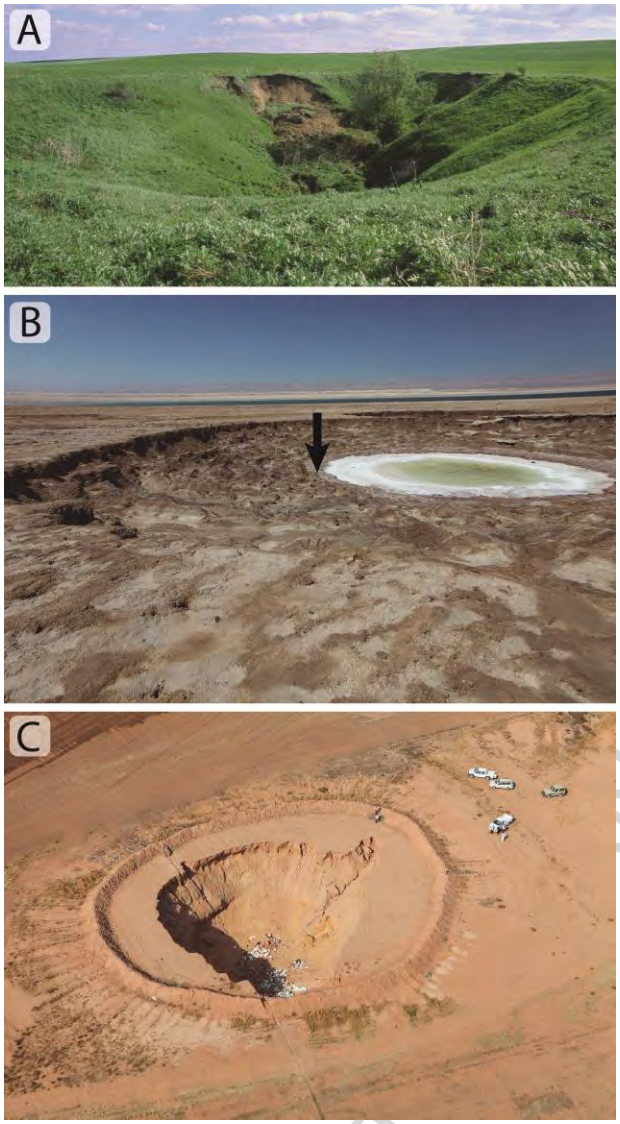


Fig. 16

Table 1. Code of samples dated by accelerator mass spectrometry, laboratory number provided by Beta Analytic, material, conventional ages and calibrated ages with an error margin of two sigma (using CALIB 7.1 and the data set IntCal 13; Reimer et al., 2013). Figures in parentheses indicate the relative area under the probability curve. More probable age ranges with relative areas larger than 50% are indicated in bold.

| Code | Laboratory number | Material | Conventional age $^{14}C$ (yr BP) | Calibrated age (2σ) (yr AD) | Calibrated age (2σ) (yr BP) |
|---|---|---|---|---|---|
| AERO-1 | Beta - 298919 | charcoal | 210± 30 | 1645 – 1683 (0.324)<br>**1734 – 1806 (0.535)**<br>1929 – 1950 (0.141) | 305 – 267 (0.324)<br>**216 – 144 (0.535)**<br>21 – 0 (0.141) |
| AERO2-1 | Beta - 299426 | charcoal | 160 ± 30 | 1664 – 1706 (0.178)<br>**1719 – 1820 (0.501)**<br>1823 – 1825 (0.004)<br>1832 – 1884 (0.132)<br>1913 – 1950 (0.184) | 286 - 244 (0.178)<br>**231 – 130 (0.501)**<br>127 – 125 (0.004)<br>118 – 66 (0.132)<br>37- 0 (0.184) |

Highlights

- Actual sinkhole extent may be much larger than that inferred by surface mapping and geophysical surveys
- Trenching allows locating precisely the edges of the subsidence areas
- Setback distances should be established considering the specific characteristics of each sinkhole
- The set-back distance typically recommend by land-use planners (ca. 15 m) may be insufficient
- Data from trenches provide the basis for reliable hazard assessment and effective risk mitigation